





Tensor-Based Method for Residual Water Suppression in ^1H Magnetic Resonance Spectroscopic Imaging

Bharath Halandur Nagaraja , Otto Debals , Diana M. Sima, Uwe Himmelreich, Lieven De Lathauwer , and Sabine Van Huffel 

I. INTRODUCTION

Abstract—Objective: Magnetic resonance spectroscopic imaging (MRSI) signals are often corrupted by residual water and artifacts. Residual water suppression plays an important role in accurate and efficient quantification of metabolites from MRSI. A tensor-based method for suppressing residual water is proposed. **Methods:** A third-order tensor is constructed by stacking the Löwner matrices corresponding to each MRSI voxel spectrum along the third mode. A canonical polyadic decomposition is applied on the tensor to extract the water component and to, subsequently, remove it from the original MRSI signals. **Results:** The proposed method applied on both simulated and in-vivo MRSI signals showed good water suppression performance. **Conclusion:** The tensor-based Löwner method has better performance in suppressing residual water in MRSI signals as compared to the widely used subspace-based Hankel singular value decomposition method. **Significance:** A tensor method suppresses residual water simultaneously from all the voxels in the MRSI grid and helps in preventing the failure of the water suppression in single voxels.

Index Terms—Canonical polyadic decomposition, magnetic resonance spectroscopic imaging, Löwner matrix, Hankel matrix, blind source separation.

Manuscript received December 22, 2017; revised April 9, 2018; accepted June 13, 2018. Date of publication July 5, 2018; date of current version January 18, 2019. The research leading to these results has received funding from the European Research Council under the European Union's Seventh Framework Programme (FP7/2007-2013) / ERC Advanced Grant: BIOTENSORS (no 339804). This paper reflects only the authors' views and the Union is not liable for any use that may be made of the contained information. This work was also supported in part by G.0830.14N (Block term decompositions) and in part by imec funds 2017. (Corresponding author: Bharath Halandur Nagaraja.)

B. Halandur Nagaraja is with the Department of Electrical Engineering, STADIUS Center for Dynamical Systems, Signal Processing and Data Analytics, KU Leuven, Leuven 3000, Belgium, and also with the IMEC, Leuven 3001, Belgium (e-mail: bhalandu@esat.kuleuven.be).

O. Debals is with the McKinsey & Company, Belgium.

D. M. Sima is with the Icometrix.

U. Himmelreich is with the Biomedical MRI Unit/Molecular Small Animal Imaging Center, Department of Imaging and Pathology, KU Leuven.

L. De Lathauwer is with the Department of Electrical Engineering, STADIUS Center for Dynamical Systems, Signal Processing and Data Analytics, KU Leuven and also with the Group of Science, Engineering and Technology, KU Leuven Kulak.

S. V. Huffel is with the Department of Electrical Engineering, STADIUS Center for Dynamical Systems, Signal Processing and Data Analytics, KU Leuven, and also with the IMEC.

This paper has supplementary downloadable material available at <http://ieeexplore.ieee.org>.

Digital Object Identifier 10.1109/TBME.2018.2850911

MAGNETIC resonance spectroscopic imaging (MRSI) is a non-invasive imaging technique that provides spectral profiles in a 2- or 3-D voxel grid, from which the spatial distribution of metabolite concentrations or metabolite ratios can be estimated. Each voxel in the MRSI grid has a spectrum composed of several peaks corresponding to the metabolites present at that location. MRSI has many clinical applications and is used, among others, to investigate psychiatric disorders [1], for diagnosis and prognosis of brain tumors [2], [3], breast cancer [4] and autism [5]. Most of the clinical applications use metabolite concentrations or metabolite ratios obtained from MRSI. Hence, an accurate and efficient quantification of metabolites is important. The metabolite levels in the human tissue are small compared to water, therefore ^1H MRSI signals typically contain a large water peak which is usually 10^3 to 10^4 larger than the metabolites of interest. This will affect the quantification of metabolites and has to be suppressed before applying any quantification algorithm. Typically, water suppression techniques are used during the acquisition of MRSI signals to get rid of large water peaks [6]. However, it is difficult to remove the water completely with these methods and some residual water will still be present in the spectra. It is important to suppress the water signal as much as possible for accurate and robust quantification of metabolites.

In general, residual water is suppressed before metabolite quantification, in a pre-processing step. Algorithms such as subspace-based Hankel singular value decomposition (HSVD) [7]–[9], multi-phase finite impulse response filtering [10], wavelet-based [11] and low rank methods based on union-of-subspaces [12] are available. Variants of these and other different methods are described in the review paper [13]. In the HSVD method, the water signal is first estimated using a subspace-based decomposition into a sum of complex damped exponentials and subsequently removed from the measured signal to suppress the water component. HSVD is the most popular residual water suppression technique and is available in many software packages such as jMRUI [14], SPID [15], VeSPA [16] and TARQUIN [11] as a preprocessing step before quantification. In MRSI, HSVD method suppress water one voxel at a time and do not exploit the shared information present among the voxels in the MRSI grid. As such, the HSVD method might

result in poor residual water suppression for some of the voxels in the MRSI grid.

Instead of using matrix-based approaches for blind source separation (BSS), there is a trend to convert the matrix data to a higher-order tensor. This transformation is called tensorization, and is part of tensor-based approaches applied to matrix data [17]. Higher-order tensors and their corresponding tools display certain properties that are not available in the matrix domain [18], [19]. Uniqueness of tensor decomposition under mild conditions is one such strong property, where additional constraints are not needed to obtain solutions as compared to the matrix case [20], [21]. In blind source separation (BSS) problems, provided the sources can be modeled or approximated by rational functions, then tensorization followed by applying tensor decompositions has better performance compared to that of the matrix based counterpart [17].

The water removal from the MRSI signals can be formulated as a blind source separation (BSS) problem. Recently, a Löwner-based BSS method has been developed, which can be used if the source signals can be approximated by rational functions. In this paper, we propose a tensor-based algorithm to suppress the residual water simultaneously from all the voxels in the MRSI signal using this Löwner-based BSS method, under the assumption that the different MRSI components can be well approximated by low-degree rational functions. We have also explored a Hankel-tensor based exponential data fitting method for water suppression. These tensor-based methods are compared against the matrix based HSVD method.

This paper is organized as follows: Section II discusses some preliminaries and the Löwner-based blind source separation and exponential data fitting using multilinear algebra. The Löwner and Hankel-based method are then applied in Section III in the MRSI water removal setting. The proposed methods are compared with HSVD using simulations and in-vivo data in Section IV. Some discussions and conclusions are presented in Section V and Section VI, respectively.

II. LÖWNER-BASED BLIND SIGNAL SEPARATION

Section II-A introduces tensors and tensor decompositions as part of multilinear algebra and fixes the notations. Löwner matrices are defined in Section II-B while Section II-C discusses the problem of blind signal separation (BSS). In Section II-D, it is shown how Löwner matrices and tensors can be used in the setting of separating (approximations by) rational functions. In Section II-E exponential data fitting using a Hankel tensor for the multichannel case is described.

A. Multilinear Algebra and Notations

1) Tensors and Notation: Tensors, denoted by calligraphic letters, e.g., \mathcal{A} , are higher-order generalizations of vectors (denoted by boldface lowercase letters, e.g., \mathbf{a}) and matrices (denoted by boldface uppercase letters, e.g., \mathbf{A}). Scalars are written as italic lowercase letters, e.g., a . The entry with row index i and column index j of a matrix $\mathbf{A} \in \mathbb{C}^{I \times J}$ is denoted by a_{ij} . Likewise, the (i_1, i_2, \dots, i_N) th entry of an N th-order tensor $\mathcal{A} \in \mathbb{C}^{I_1 \times I_2 \times \dots \times I_N}$ is denoted by $a_{i_1 i_2 \dots i_N}$. The j th column of

a matrix $\mathbf{A} \in \mathbb{C}^{I \times J}$ is denoted by \mathbf{a}_j . The superscripts \cdot^T , \cdot^H , \cdot^{-1} and \cdot^\dagger represent the transpose, complex conjugated transpose, inverse and pseudo inverse, respectively. The symbol \otimes and \circ denotes the outer product and Hadamard product, respectively.

2) Tensor Decompositions: A tensor \mathcal{T} has rank 1 if it can be written as the outer product of some nonzero vectors: $\mathcal{T} = \mathbf{a}^{(1)} \otimes \mathbf{a}^{(2)} \otimes \dots \otimes \mathbf{a}^{(N)}$. If \mathcal{T} is written as a linear combination of R rank-1 tensors, one obtains a Polyadic Decomposition (PD):

$$\mathcal{T} = \sum_{r=1}^R \mathbf{a}_r^{(1)} \otimes \dots \otimes \mathbf{a}_r^{(N)} \triangleq \left[\mathbf{A}^{(1)}, \dots, \mathbf{A}^{(N)} \right].$$

If R is minimal, the decomposition becomes canonical (CPD) and the rank of \mathcal{T} is defined as R .

Another decomposition is the low multilinear rank approximation (LMLRA) [22]. One way of calculating an LMLRA is through the multilinear singular value decomposition (MLSVD) [23]. A tensor \mathcal{T} can then be written as the tensor-matrix product of a typically smaller core tensor \mathcal{S} with N factor matrices $\mathbf{U}^{(n)}$, $n = 1, \dots, N$, along the different modes. For more details on tensors and tensor decompositions, we refer the interested reader to [18], [19], [24].

3) Computation of Tensor Decompositions: Given a tensor \mathcal{T} , there are a number of algorithms available to find the rank-1 terms of \mathcal{T} . The most popular one is the alternating least squares (ALS) method, whereas a more advanced algorithm is the nonlinear least squares (NLS) method. Two commonly used initialization methods are random initializations and a technique based on the generalized eigenvalue decomposition (GEVD) [25].

The approach in this paper makes use of a compression step and a CPD step [26]. The compression step applies an MLSVD with truncation to compute a smaller core tensor \mathcal{S} and corresponding factor matrices $\mathbf{U}^{(n)}$. Provided that the dimensions of \mathcal{S} exceed R , it can be shown that \mathcal{S} still has (approximately) rank R if \mathcal{T} has (approximately) rank R . In the second step, a CPD is performed on the smaller tensor \mathcal{S} (rather than on \mathcal{T}), which returns the factor matrices $\mathbf{B}^{(n)}$. The n th factor matrix of \mathcal{T} is then equal to $\mathbf{A}^{(n)} = \mathbf{U}^{(n)} \mathbf{B}^{(n)}$. This two-step procedure is especially beneficial if \mathcal{T} is large, as the computation complexity of the CPD algorithm is higher compared to the MLSVD algorithm. If \mathcal{T} only approximately has rank R , the two-step procedure still provides good estimates in various occasions which differ only minimally compared to the estimates from computing a CPD on \mathcal{T} directly.

B. Löwner and Hankel Matrices/Tensors

While the concept of Löwner matrices is highly acknowledged in the domain of system identification [27], [28], it is not well known in other application domains. In a recent study, Löwner matrices have been used in a BSS context to separate (approximations by) rational functions [17].

Suppose a function $f(t) \in \mathbb{C}$ is given, evaluated in the point set $T = \{t_1, t_2, \dots, t_N\}$. The point set T is partitioned into two distinct point sets, $X = \{x_1, x_2, \dots, x_I\}$ and $Y = \{y_1, y_2, \dots, y_J\}$ with $I + J = N$. The elements of the Löwner

matrix $\mathbf{L} \in \mathbb{C}^{I \times J}$ are then defined as

$$\forall i, j: l_{ij} = \frac{f(x_i) - f(y_j)}{x_i - y_j}.$$

We thus obtain the following matrix:

$$\mathbf{L} = \begin{bmatrix} \frac{f(x_1) - f(y_1)}{x_1 - y_1} & \frac{f(x_1) - f(y_2)}{x_1 - y_2} & \cdots & \frac{f(x_1) - f(y_J)}{x_1 - y_J} \\ \frac{f(x_2) - f(y_1)}{x_2 - y_1} & \frac{f(x_2) - f(y_2)}{x_2 - y_2} & \cdots & \frac{f(x_2) - f(y_J)}{x_2 - y_J} \\ \vdots & \vdots & \ddots & \vdots \\ \frac{f(x_I) - f(y_1)}{x_I - y_1} & \frac{f(x_I) - f(y_2)}{x_I - y_2} & \cdots & \frac{f(x_I) - f(y_J)}{x_I - y_J} \end{bmatrix}.$$

Given K functions $f_i(t)$ evaluated on the same set of N points, a Löwner matrix \mathbf{L}_i can be computed for each function. By stacking the different matrices \mathbf{L}_i in a tensor along the third mode, a Löwner tensor $\mathcal{L} \in \mathbb{C}^{I \times J \times K}$ is obtained.

Hankel matrices are used in many applications such as system identification, coding theory. For a function $f(t) \in \mathbb{C}$ evaluated at N distinct points $T = \{t_1, t_2, \dots, t_N\}$, the elements of a $I \times J$ Hankel matrix with $I + J - 1 = N$ are defined as

$$\forall i, j: h_{ij} = f(t_{i+j-1}).$$

and in matrix form it is represented as:

$$\mathbf{H} = \begin{bmatrix} f(t_1) & f(t_2) & \cdots & f(t_{J-1}) & f(t_J) \\ f(t_2) & f(t_3) & \cdots & f(t_J) & f(t_{J+1}) \\ \vdots & \vdots & \ddots & \vdots & \vdots \\ f(t_{I-1}) & f(t_I) & \cdots & f(t_{I+J-3}) & f(t_{I+J-2}) \\ f(t_I) & f(t_{I+1}) & \cdots & f(t_{I+J-2}) & f(t_{I+J-1}) \end{bmatrix}.$$

Similar to the Löwner tensor, a Hankel tensor $\mathcal{H} \in \mathbb{C}^{I \times J \times K}$ can be constructed from K functions $f_i(t)$ by stacking the Hankel matrices \mathbf{H}_i in a tensor along the third mode.

C. Blind Source Separation

Given a set of observed signals $\mathbf{S} \in \mathbb{C}^{N \times K}$, the BSS problem consists of identifying the mixing matrix $\mathbf{H} \in \mathbb{C}^{K \times R}$ and/or the original source signals in $\mathbf{W} \in \mathbb{C}^{N \times R}$ based on the following linear model:

$$\mathbf{S} = \mathbf{W}\mathbf{H}^T, \quad (1)$$

with K the number of observed signals, R the number of source signals and N the number of samples per signal. By itself, the solution cannot be uniquely identified as different working hypotheses lead to different solutions (at least for the non-trivial cases $R > 1$). Different working assumptions have been used before such as mutual independence of the source signals which leads to independent component analysis. In this paper, we use a deterministic approach with the assumption that each source can be well approximated by a rational function as discussed in the next section.

D. Löwner-Based Blind Source Separation of (Approximations by) Rational Functions

Rational functions are formed by algebraic fractions with polynomials in the numerator and denominator. We limit the discussion in this paper to rational functions of degree 1, meaning that the numerator and denominator are linear functions. This is a special case of the technique developed in [17] for arbitrary degree.

If \mathbf{L} is a Löwner matrix constructed by a rational function of degree 1, it has been proven that \mathbf{L} has rank 1 [27], [29]. This is easy to verify: $f(t) = \frac{c}{t-p}$ gives $L_{i,j} = -c \cdot \frac{1}{x_i - p} \cdot \frac{1}{y_j - p}$, which is a rank-1 structure:

$$\mathbf{L} = -c \cdot \begin{bmatrix} \frac{1}{x_1 - p} \\ \vdots \\ \frac{1}{x_I - p} \end{bmatrix} \begin{bmatrix} \frac{1}{y_1 - p} & \cdots & \frac{1}{y_J - p} \end{bmatrix}.$$

Consider now the construction of two tensors $\mathcal{L}_S \in \mathbb{C}^{I \times J \times K}$ and $\mathcal{L}_W \in \mathbb{C}^{I \times J \times N}$. The tensors \mathcal{L}_S and \mathcal{L}_W contain Löwner matrices along the third mode constructed from the observed signals from \mathbf{S} , and the source signals from \mathbf{W} , respectively. Following the linear model (1), the tensor \mathcal{L}_S can be expressed as

$$\mathcal{L}_S = \sum_{r=1}^R \mathbf{L}_{w_r} \otimes \mathbf{h}_r. \quad (2)$$

If each source signal is an evaluated rational function (or can be approximated by an evaluated rational function), each matrix \mathbf{L}_{w_r} has (approximately) rank 1 [17]. Hence, each term in (2) has (approximately) rank 1 and the tensor \mathcal{L}_S has CPD structure with rank R .

To solve the BSS problem from (1) under the deterministic assumption of rationality, a CPD can be computed of \mathcal{L}_S with rank R . The factor matrix $\hat{\mathbf{H}}$ in the third mode is then an estimate of the mixing matrix \mathbf{H} . The source signals can be recovered as $\hat{\mathbf{W}} = \mathbf{S}(\hat{\mathbf{H}}^T)^\dagger$. Alternatively, estimates of the source signals

can be obtained from the estimated matrices $\hat{\mathbf{L}}_{w_r}$. Note that the two indeterminacies of BSS are consistent with the indeterminacies of the CPD: the source signals (factor vectors) are recovered up to permutation and scaling.

It remains to show that the separation is unique. This property guarantees that the recovered source signals are (estimates of) the original source signals. This uniqueness problem boils down to the CPD uniqueness given the special rational structure of the factor vectors. In [17, Theorem 4], it has been proven that if the poles of the rational functions of the different source signals are distinct and if N is sufficiently large, the CPD is unique (up to permutation and scaling of the factor vectors) given that \mathbf{H} does not contain proportional columns. Note that uniqueness can still be guaranteed for underdetermined mixtures with fewer observed signals than source signals. Generic conditions for the BSS settings are given in [30].

E. Hankel-Based Exponential Data Fitting

For the blind BSS problem in (1), if each of the observed signals are modeled as a sum of complex exponentials $\mathbf{s}_k = \sum_{r=1}^{\hat{R}} c_{kr} z_{kr}^n, \forall n = \{0, 1, \dots, N-1\}$, a Hankel-based exponential data fitting method can be applied for estimating the source and mixing matrix [31]. A tensor $\mathcal{H} \in \mathbb{C}^{I \times J \times K}$ constructed by stacking K Hankel matrices obtained from columns of \mathbf{S} can be decomposed as follows:

$$\mathcal{H} = \sum_{r=1}^R \begin{bmatrix} 1 \\ z_r^1 \\ z_r^2 \\ \vdots \\ z_r^J \end{bmatrix} \otimes \begin{bmatrix} 1 \\ z_r^1 \\ z_r^2 \\ \vdots \\ z_r^J \end{bmatrix} \otimes \begin{bmatrix} c_{1r} \\ c_{2r} \\ c_{3r} \\ \vdots \\ c_{kr} \end{bmatrix}. \quad (3)$$

$$\mathcal{H} = \mathcal{I} \times_1 \mathbf{V}^{(1)} \times_2 \mathbf{V}^{(2)} \times_3 \mathbf{C},$$

where \times_n is the n -mode product of a tensor by a matrix [23], \mathcal{I} is a pseudo-diagonal $(R \times R \times R)$ -tensor with ones on its diagonal, $\mathbf{V}^{(1)} \in \mathbb{C}^{I \times R}$, $\mathbf{V}^{(2)} \in \mathbb{C}^{J \times R}$ are Vandermonde matrices and $\mathbf{C} \in \mathbb{C}^{K \times R}$ contains the complex amplitudes. A $I \times R$ Vandermonde matrix \mathbf{V} with z_1, \dots, z_R as generators is defined as:

$$\mathbf{V} = \begin{bmatrix} 1 & 1 & \dots & 1 \\ z_1 & z_2 & \dots & z_1 \\ z_1^2 & z_2^2 & \dots & z_1^2 \\ \vdots & \vdots & \ddots & \vdots \\ z_1^{I-1} & z_2^{I-1} & \dots & z_1^{I-1} \end{bmatrix}$$

Vandermonde decomposition is difficult to estimate. However, a similar decomposition can be obtained by applying truncated MLSVD to the Hankel tensor \mathcal{H}

$$\mathcal{H} = \mathcal{A} \times_1 \mathbf{U}^{(1)} \times_2 \mathbf{U}^{(2)} \times_3 \mathbf{U}^{(3)}. \quad (4)$$

where \mathcal{A} is an all-orthogonal, ordered, complex $(R \times R \times R)$ -tensor, $\mathbf{U}^{(1)} \in \mathbb{C}^{I \times R}$ is a complex matrix of which the orthonormal columns span the column space of $\mathbf{V}^{(1)}$, $\mathbf{U}^{(2)} \in \mathbb{C}^{J \times R}$ is a complex matrix of which the orthonormal columns span the column space of $\mathbf{V}^{(2)}$ and $\mathbf{U}^{(3)} \in \mathbb{C}^{K \times R}$ is a complex matrix of which the orthonormal columns span the column space of \mathbf{C} . Because of an underlying isomorphism between equation (3) and (4), the matrices $\mathbf{U}^{(p)}$ are related to matrices $\mathbf{V}^{(p)}$ ($p = 1, 2$) by a non-singular matrix \mathbf{Q}

$$\mathbf{U}^{(p)} = \mathbf{V}^{(p)} \mathbf{Q}. \quad (5)$$

Signal poles z_r can be determined using the shift-invariance property of Vandermonde matrices [31]:

$$\mathbf{V}^{(p)\uparrow} = \mathbf{V}_\downarrow^{(p)} \mathbf{Z}, \quad (6)$$

where the up and down arrow placed after a matrix stands for deleting the top and bottom row of the considered matrix, respectively and \mathbf{Z} is a diagonal matrix with signal poles z_r along

the diagonal. Combining equations (5) and (6) result in the shift-invariance property of the MLSVD factor matrices $\mathbf{U}^{(p)}$

$$\mathbf{U}^{(p)\uparrow} = \mathbf{U}_\downarrow^{(p)} \hat{\mathbf{Z}},$$

with $\hat{\mathbf{Z}} = \mathbf{Q}^{-1} \mathbf{Z} \mathbf{Q}$. The matrices \mathbf{Z} and $\hat{\mathbf{Z}}$ have the same eigenvalues. A least squares solution is used to estimate $\hat{\mathbf{Z}} = (\mathbf{U}_\downarrow^{(p)})^\dagger \mathbf{U}^{(p)\uparrow}$. Finally, the signal poles z_r are obtained from the eigen-decomposition of $\hat{\mathbf{Z}}$. A Vandermonde source matrix is constructed from the estimated signal poles and the mixing matrix \mathbf{H} can then be estimated using least squares.

III. LÖWNER-BASED METHOD FOR WATER REMOVAL

Section III-A explains the MRSI and the water signal model. Section III-B discusses blind source separation of MRSI signals and in Section III-B2, estimation of source parameters obtained from BSS is explained. Section III-B3 describes the extraction of the water component from the MRSI data.

A. MRSI and Residual Water

The MRSI time-domain signal is represented by a free-induction (FID). The complex time-domain FID signal in each voxel can be modeled by a sum of complex damped exponentials:

$$F(t) = \sum_{r=1}^R a_r e^{j\phi_r} e^{(-d_r + j2\pi f_r)t},$$

in which R is the number of resonance peaks in the signal, and f_r , a_r , ϕ_r and d_r are the frequency, amplitude, phase and damping of the r^{th} resonance peak, respectively. Similarly, in the frequency domain, the Fourier transform of the FID signal can be modeled as a sum of rational functions.

$$S(f) = \sum_{r=1}^R \frac{a_r e^{j\phi_r} / 2\pi}{d_r + j2\pi(f - f_r)} = \sum_{r=1}^R \frac{c_r}{j\omega + p_r}, \quad (7)$$

where $c_r = a_r e^{j\phi_r} / 2\pi$ is the complex amplitude, $p_r = d_r - j2\pi f_r$ is the complex pole and $\omega = 2\pi f$ is the angular frequency.

The MRSI data matrix \mathbf{S} is constructed by stacking the spectra from each voxel in the columns. Similarly, the data matrix \mathbf{F} is defined by stacking the FID's from each voxel. The residual water present in the MRSI signals is sometimes large and can strongly affect the metabolite peaks of interest, which belong to the region of interest in 0.25–4.2 ppm as shown in Fig. 1. In theory, the water signal can be represented by only one exponential/rational function in time/frequency domain, but this model is not sufficient for an in-vivo signal. In practice, it is possible to model the residual water signal with a linear combination of several exponentials [8], which can then be extracted from \mathbf{S} (respectively, \mathbf{F}).

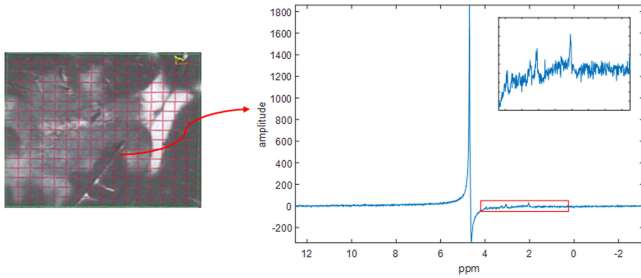


Fig. 1. Magnitude of the absorption spectra from one of the voxels in the MRSI grid with a large residual water signal. The region of interest for metabolites is shown within the red box.

B. Löwner-Based Water Suppression

1) **Löwner-Based Blind Source Separation in MRSI:** It has been shown in [8] that it is possible to model the in-vivo residual water signal with a linear combination of several exponentials. Here, we assume that neighboring voxels in the MRSI signal share sources (rank-1 rational functions) that are used to model the residual water signal. Hence, the estimation of sources that model residual water and their corresponding abundances from the K measured MRSI signals can be formulated as a BSS problem:

$$\mathbf{S} = \mathbf{W}\mathbf{H}^T,$$

where columns of $\mathbf{S} \in \mathbb{C}^{N \times K}$ contain the measured spectra from all the voxels, the columns of $\mathbf{W} \in \mathbb{C}^{N \times R}$ represent the individual metabolite components and the columns of $\mathbf{H} \in \mathbb{C}^{K \times R}$ (the mixing matrix) represent their corresponding abundances (weights) in each voxel. We use the Löwner-based BSS technique explained in Section II-D to estimate the individual metabolite sources. For each voxel, a Löwner matrix \mathbf{L}_{S_k} is constructed from the corresponding spectrum in the MRSI grid:

$$\mathbf{L}_{S_k} = \begin{bmatrix} \frac{S_k(x_1) - S_k(y_1)}{x_1 - y_1} & \frac{S_k(x_1) - S_k(y_2)}{x_1 - y_2} & \cdots & \frac{S_k(x_1) - S_k(y_J)}{x_1 - y_J} \\ \frac{S_k(x_2) - S_k(y_1)}{x_2 - y_1} & \frac{S_k(x_2) - S_k(y_2)}{x_2 - y_2} & \cdots & \frac{S_k(x_2) - S_k(y_J)}{x_2 - y_J} \\ \vdots & \vdots & \ddots & \vdots \\ \frac{S_k(x_I) - S_k(y_1)}{x_I - y_1} & \frac{S_k(x_I) - S_k(y_2)}{x_I - y_2} & \cdots & \frac{S_k(x_I) - S_k(y_J)}{x_I - y_J} \end{bmatrix},$$

in which S_k is the spectrum of the k th voxel, and with $\{x_1, \dots, x_I\}$ and $\{y_1, \dots, y_J\}$ two partitions of the point set $\Omega = \{\omega_1, \dots, \omega_N\}$ with $N = I + J$. Two typical partitioning types for Ω are interleaved and block partitioning. Interleaved partition was used for constructing the Löwner matrix in this paper.

The Löwner matrix is constructed using the spectrum from 0.25–6.5 ppm, which contains the region of interest in 0.25–4.2 ppm and the water region. A third-order tensor \mathcal{L}_S is obtained by stacking the Löwner matrices along the third mode as shown in Fig. 2.

As it is assumed that each individual component \mathbf{w}_r can be well approximated by a degree-1 rational function with a single resonance peak as described in (7), each corresponding r th Löwner matrix has approximately rank 1 and can be described

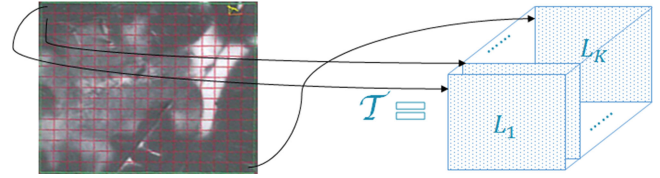


Fig. 2. Construction of the Löwner tensor \mathcal{T} from the spectra of the different MRSI voxels.

as $\mathbf{a}_r \mathbf{b}_r^T$. Hence, a CPD can be applied on \mathcal{L}_S :

$$\mathcal{L}_S \approx \sum_{r=1}^R \mathbf{a}_r \otimes \mathbf{b}_r \otimes \mathbf{h}_r = \llbracket \mathbf{A}, \mathbf{B}, \mathbf{H} \rrbracket, \quad (8)$$

with $\mathbf{A} \in \mathbb{C}^{I \times R}$, $\mathbf{B} \in \mathbb{C}^{J \times R}$ and $\mathbf{H} \in \mathbb{C}^{K \times R}$. Each rank-1 tensor corresponds to the contribution of a particular component to the observed spectral data.

2) **Estimation of Source Parameters:** The abundance vectors \mathbf{h}_r can be directly identified from (8). A second goal is to identify the source components and their corresponding parameters as described in (7). The r th source is modeled by $\mathbf{w}_r(\omega) = \frac{c_r}{j\omega + p_r}$, and its corresponding Löwner matrix \mathbf{L}_{w_r} can be written as:

$$\begin{aligned} \mathbf{L}_{w_r} &= \begin{bmatrix} \frac{-jc_r}{(jx_1 + p_r)(jy_1 + p_r)} & \frac{-jc_r}{(jx_1 + p_r)(jy_2 + p_r)} & \cdots & \frac{-jc_r}{(jx_1 + p_r)(jy_J + p_r)} \\ \frac{-jc_r}{(jx_2 + p_r)(jy_1 + p_r)} & \frac{-jc_r}{(jx_2 + p_r)(jy_2 + p_r)} & \cdots & \frac{-jc_r}{(jx_2 + p_r)(jy_J + p_r)} \\ \vdots & \vdots & \ddots & \vdots \\ \frac{-jc_r}{(jx_I + p_r)(jy_1 + p_r)} & \frac{-jc_r}{(jx_I + p_r)(jy_2 + p_r)} & \cdots & \frac{-jc_r}{(jx_I + p_r)(jy_J + p_r)} \end{bmatrix} \\ &= \begin{bmatrix} \frac{c_r^{(1)}}{jx_1 + p_r} \\ \frac{c_r^{(1)}}{jx_2 + p_r} \\ \vdots \\ \frac{c_r^{(1)}}{jx_I + p_r} \end{bmatrix} \begin{bmatrix} \frac{c_r^{(2)}}{jy_1 + p_r} & \frac{c_r^{(2)}}{jy_2 + p_r} & \cdots & \frac{c_r^{(2)}}{jy_J + p_r} \end{bmatrix} \\ &= \mathbf{a}_r \mathbf{b}_r^T \end{aligned}$$

with $-jc_r = c_r^{(1)} c_r^{(2)}$. The parameters $c_r^{(1)}$ and p_r can be obtained from \mathbf{a}_r using least squares,

$$\begin{bmatrix} p_r \\ c_r^{(1)} \end{bmatrix} = [\mathbf{a}_r \quad -\mathbf{1}]^\dagger (j\mathbf{x} \circ \mathbf{a}_r),$$

where $\mathbf{1} \in \mathbb{R}^I$ is the vector with all ones. We can estimate $c_r^{(2)}$ and p_r from \mathbf{b}_r in a similar way. The final estimate of p_r can be obtained by averaging the estimates from \mathbf{a}_r and \mathbf{b}_r .

3) **Water Signal Suppression:** Once the source parameters are estimated, the model is extrapolated to the entire length of the frequency region. The abundance matrix \mathbf{H} is calculated using least squares from the source signals and measured spectra, $\mathbf{H} = (\mathbf{W}^\dagger \mathbf{S})^T$. The real part of each estimated pole gives the damping factor of the corresponding source (d_r) while the

imaginary part returns the resonance frequency. The components whose resonance frequencies are outside the region of interest (0.25 - 4.2 ppm) belong to the water component or provide other nuisance peaks. Therefore, the influence of the water component on the observed spectral data is constructed using only those components and their corresponding abundance vectors. Let Φ denote the set of P indices corresponding to the P water sources. Then $\mathbf{W}_{water} = [\mathbf{w}_{\Phi_1} \cdots \mathbf{w}_{\Phi_P}]$ and $\mathbf{H}_{water} = [\mathbf{h}_{\Phi_1} \cdots \mathbf{h}_{\Phi_P}]$, and the contribution of the water component can be expressed as $\mathbf{S}_{water} = \mathbf{W}_{water} \mathbf{H}_{water}^T$. The water component can then be removed from the measured MRSI spectra as $\mathbf{S}_{suppressed} = \mathbf{S} - \mathbf{S}_{water}$.

After removing the water component from the MRSI signal, a small baseline will be present at the outer edges of the spectrum. This arises mainly because the Löwner method is not able to model the complex water signal properly at the outer edges of the spectrum when the water signal has some baseline. Also damped complex exponential function translates to rational function only when signal is continuous and infinitely long. The HSVD method can estimate a source with a broad peak (large damping) to model the edges of the water spectrum, whereas Löwner method fails to extract such broad peaks and hence fails to model the water spectrum at the outer edges and results in a baseline. This problem can be corrected by modeling the baseline using a polynomial function of degree D . Therefore, the polynomial functions are added to the estimated source matrix \mathbf{W} to obtain the matrix $\mathbf{W}_{poly} \in \mathbb{R}^{N \times (K+d+1)}$:

$$\mathbf{W}_{poly} = \begin{bmatrix} w_{11} & w_{12} & \cdots & w_{1R} & 1 & f_1 & f_1^2 & \cdots & f_1^d \\ w_{21} & w_{22} & \cdots & w_{2R} & 1 & f_2 & f_2^2 & \cdots & f_2^d \\ \vdots & \vdots & \ddots & \vdots & \vdots & \vdots & \vdots & \ddots & \vdots \\ w_{N1} & w_{N2} & \cdots & w_{NR} & 1 & f_N & f_N^2 & \cdots & f_N^d \end{bmatrix}$$

The abundance matrix \mathbf{H} is recalculated in a least-squares sense using the estimate of \mathbf{W}_{poly} and the measured spectra in \mathbf{S} . The residual water component is suppressed using the subtraction method as explained above. Each polynomial source is also considered as a water component.

In this method the water signal in each voxel is modeled as a linear combination of many (resonance peaks/rank-1 rational functions) (typically 20–30). For each voxel, the rows of the abundance matrix \mathbf{H} specify the subset of sources that are used to model the water signal by means of their corresponding weights. Since these weight combinations are voxel-wise different, they can model voxel-wise variations in the water component. This will allow to handle the B0 inhomogeneity and spectrum distortions present in the MRSI signals.

The CPD algorithm requires an initial value for the factor matrices. Random initializations can sometimes result in poor water suppression. In order to overcome this problem, different initializations are used if the water suppression is not sufficient. To verify the quality of the water suppression, the variance in the water region and noise region are compared. If the variance in the water segment is larger than the variance in the noise segment by a given threshold, the water suppression is considered to be

poor and a different initial value is used until a good suppression is obtained.

C. Hankel-Tensor Based Water Suppression in MRSI

In the time domain the BSS problem of separating individual resonance peaks can be formulated as:

$$\mathbf{F} = \mathbf{V} \mathbf{H}^T, \quad (9)$$

where columns of $\mathbf{F} \in \mathbb{C}^{N \times K}$ contain the measured FID from all the voxels, $\mathbf{V} \in \mathbb{C}^{N \times R}$ is the Vandermonde matrix of the R source poles (z_r) and the columns of $\mathbf{H} \in \mathbb{C}^{K \times R}$ (the mixing matrix) represent their corresponding abundances (weights) in each voxel.

Similarly to the Löwner method, for each voxel a Hankel matrix \mathbf{H}_{f_k} is constructed from the corresponding time-domain FID signal. A third-order tensor \mathcal{H}_f is obtained by stacking the Hankel matrices along the third mode as shown in Fig. 2. We can estimate the poles $z_r = e^{-d_r + 2\pi f_r}$ of the MRSI signals by applying MLSVD to the Hankel tensor \mathcal{H}_f as explained in Section II-E. The abundance matrix \mathbf{H} is then calculated using the least squares solution of the equation (9) in which the Vandermonde matrix V is derived from the estimated poles, $\mathbf{H} = (\mathbf{V}^\dagger \mathbf{F})^T$. The real part of each $\log(z_r)$ gives the damping factor of the corresponding source (d_r) while the imaginary part returns the resonance frequency. The components with resonance frequencies outside the region of interest (0.25 - 4.2 ppm) are considered to reconstruct the water component and possibly other nuisance peaks. Finally, the residual water is suppressed from the MRSI signal by subtracting the estimated water component similarly to the Löwner method.

IV. RESULTS

To test the performance of the Löwner and Hankel-tensor based water suppression methods, they are applied on both simulated and in-vivo MRSI data. Section IV-C discusses the performance of the Löwner, the Hankel-tensor and the HSVD methods on simulated datasets. In Section IV-D the performance of the Löwner, Hankel-tensor and HSVD methods is assessed using in-vivo data. Tensorlab is used for the Löwner and Hankel matrix constructions and tensor computations [32], [33]. The signal-to-noise ratio (SNR) is defined as the power of the signal to the power of the noise. Unless stated otherwise, a rank $R = 50$ is used for the CPD of the Löwner tensor \mathcal{L}_s and $d = 4$ degree polynomial sources are used for the entire MRSI in both the simulation and in-vivo cases. For the HSVD, an order of 50 was used for each voxel and for Hankel-tensor we have used an order of 100 in the MLSVD of the entire MRSI signal.

A. Materials

A total of 28 2-D-¹H MRSI data was acquired on a 3T MR scanner (Achieva, Philips, Best, The Netherlands) at the University Hospital of Leuven from brain tumour patients. The study and the experimental procedures involving human subjects have been approved by the ethical committee of the institute. The following protocol [34] was used for the acquisition: a

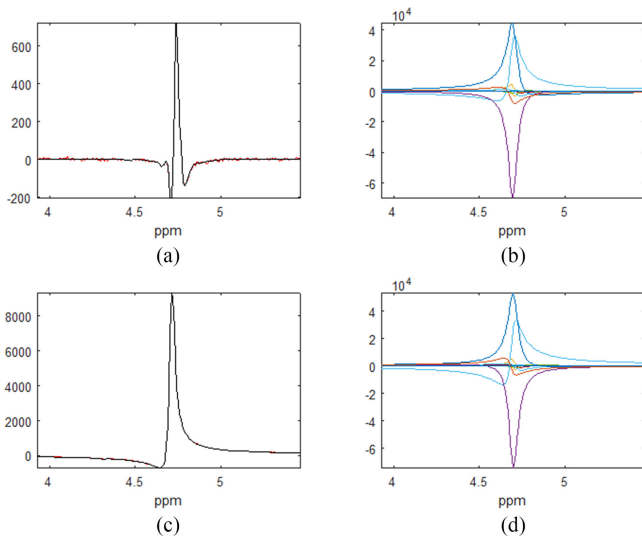


Fig. 3. (a) & (c) Absorption spectra of an in-vivo signal without water suppression (red, dashed-line) overlapped with the estimated water spectra (black, solid-line) from two different voxels in the MRSI grid. (b) & (d) Individual resonance peaks used in the modelling of the water signal from (a) and (c), respectively.

point-resolved spectroscopy (PRESS) sequence was used as the volume selection technique with a bandwidth of 1.3 kHz for the conventional slice-selective pulses; repetition time (TR)/echo time (TE): 2000/35 ms; Field of view (FOV): $160 \times 160 \text{ mm}^2$; maximal volume of interest (VOI): $80 \times 80 \text{ mm}^2$; slice thickness: 10 mm; acquisition voxel size: $10 \times 10 \text{ mm}^2$; reconstruction voxel size: $5 \times 5 \text{ mm}^2$; receiver bandwidth: 2000 Hz; samples: 2048; number of signal averages: 1; water suppression method: multiple optimizations insensitive suppression train (MOIST) [6]; first- and second-order pencil beam shimming; parallel imaging: sensitivity encoding with reduction factors of 2 (left-right) and 1.8 (anterior-posterior); scan time: around 3 min 30 s. Automated prescanning optimized the shim in order to yield a peak width consistently under 20 Hz full-width half-maximum (FWHM). Voxels outside the MRSI PRESS excitation volume are excluded from the analysis.

B. Spectral Variations in MRSI Voxels

To demonstrate that our proposed method can handle B0 inhomogeneity and spectrum distortions, we have applied the Löwner method to one in-vivo dataset. Fig. 3(a) & (c) shows absorption spectra of an in-vivo MRSI signal from two of the voxels having different spectral shape (red, dashed-line). The estimated water signal (black, solid-line) is overlapped on the measured spectrum in the figure, and we can clearly see that the estimated water signal (black, solid line) models both voxels that are having distinct spectral shapes. Fig. 3(b) & (d) show the individual resonance peaks used to model the water signal. From the figure we can observe that the individual resonance peaks used to model the water component have different complex amplitude for both voxels, which enables to handle B0 inhomogeneity and spectral distortions.

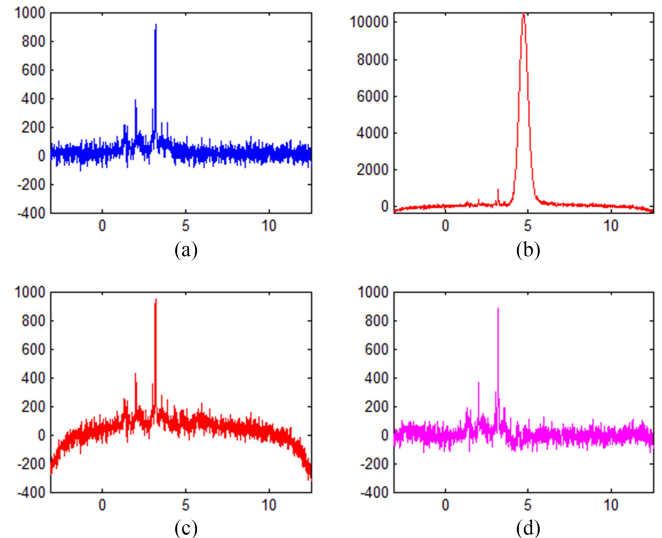


Fig. 4. (a) Absorption spectrum of a simulated in-vitro signal without water from one of the MRSI voxels. (b) Absorption spectrum of a simulated in-vitro signal with large water peak from one of the MRSI voxels. (c) Absorption spectrum of the water-suppressed signal using the Löwner method without polynomial sources. (d) Absorption spectrum of the water-suppressed signal using the Löwner method with polynomial sources.

C. Simulations

The simulated signals containing residual water are generated using an in-vitro basis set which was obtained as described in [35]. The basis set consisting of in-vitro signals from Alanine (Ala), Aspartate (Ala), Choline (Cho), Creatine (Cre), γ -aminobutyric acid (GABA), Glutamate (Glu), Lactate (Lac), two lipids (Lip1 and Lip2), myo-Inositol (MI), N-Acetyl-Aspartate (NAA) and Taurine (Tau) metabolites was used to generate the spectra. A grid of MRSI signals of size 16×16 was generated for simulation. First, signals consisting of 12 metabolites are constructed using the basis set without any residual water. The amplitude of each metabolite in the grid is varied using a 2-D Gaussian window,

$$g(x, y) = e^{-(x^2+y^2)/2\sigma^2} + U(x, y)$$

where $U(x, y)$ is a uniformly distributed random number, and $x = 0, y = 0$ is the central voxel. Circular Gaussian noise is added to the metabolite signals. Residual water signal was generated by scaling the in-vitro measured MRSI water reference signal. In each voxel the residual water signal is distorted by multiplying it with a Gaussian decaying signal $e^{-d_k t^2}$, where d_k is modelled as a uniformly distributed random variable between 0 and 0.005. Finally, residual water was added to the noisy metabolite signals to generate the MRSI data.

The Löwner method with and without polynomial sources was applied on a simulated MRSI signal to suppress the residual water. The result of water removal in one of the voxels is shown in Fig. 4. From Fig. 4(c) & (d) we can clearly observe that the Löwner method will introduce a baseline and it can be addressed by including the polynomial sources in the least squares stage. In the remainder of the paper, we have only considered the Löwner method with polynomial sources, unless explicitly mentioned.

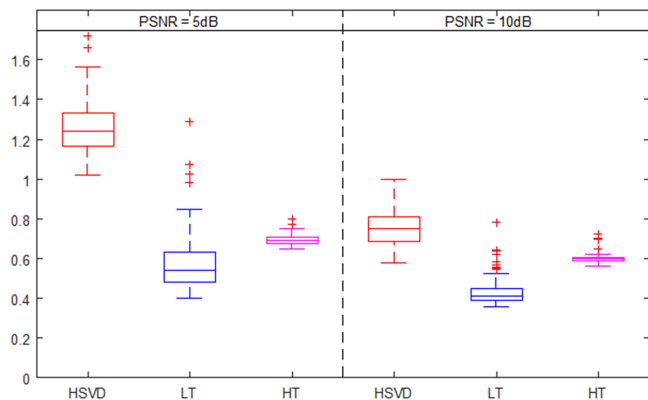


Fig. 5. Boxplot of the residual errors after water suppression using the HSVD, the Löwner (LT), and the Hankel-tensor (HT) methods on 100 simulated in-vitro MRSI signals. The error is calculated as the l_2 -norm of the difference between the water-suppressed signal and the original water-free signal (with noise).

The Löwner, Hankel-tensor and HSVD water-suppression methods are applied on the simulated MRSI signals for 100 different noise and metabolite amplitude realizations. Fig. 5 shows the boxplot of errors between the water-suppressed signal and the metabolite signal (with noise) for two different noise levels. The boxplot indicates that both the Löwner-based method and the Hankel-tensor method have a lower average error compared to the HSVD method and suppresses the residual water better without distorting the metabolite spectra. The Löwner-based method has the best performance in suppressing residual water compared to other two methods.

D. In-Vivo Results

To test the performance of the algorithms we have applied the HSVD, Hankel tensor and Löwner methods on 28 in-vivo datasets. Fig. 6 shows the real part of the spectra with residual water and after water suppression for two different voxels in a MRSI grid. In many voxels, all three methods give good water suppression as shown in Fig. 6(c). However, in some voxels the HSVD method does not perform well as shown in Fig. 6(f). In Fig. 6(b), we can observe that an artefact is present at the right side of the water signal. Therefore the HSVD method fails to suppress water completely and results in a significant residue. However, both tensor methods are able to suppress water even in the presence of an artefact.

There is no ground truth available for in-vivo data to measure the quality of water suppression. To measure the performance, we calculate the difference in sample variance between the water region segment and the noise segment in each voxel. The spectrum in the region of 4.2–5.2 ppm is considered as water segment and the spectrum at the outer edges is considered as noise segment. For each MRSI signal, the average difference in variance is used as the performance measure. Fig. 7 shows the boxplot of sample variance difference of 28 MRSI in-vivo data signals for the HSVD, Hankel tensor and Löwner methods.

Next, we tried to analyse the quality of water suppression by quantifying MRSI signals and examining the Cramer Rao bounds of the metabolite amplitudes. Two in-vivo MRSI signals

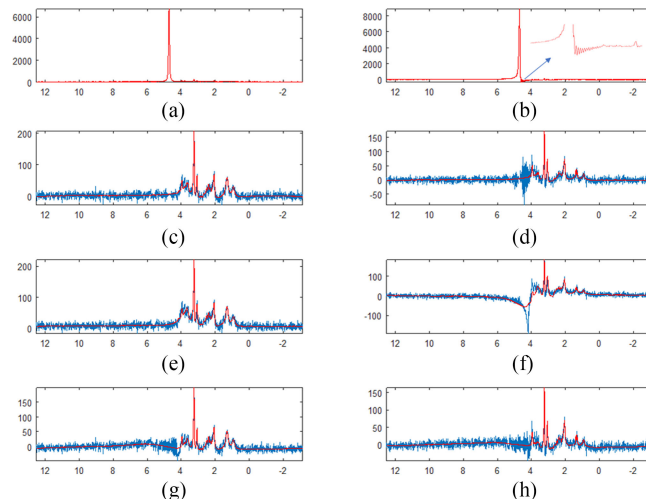


Fig. 6. Residual water suppression in in-vivo MRSI signals. (a)–(b) Absorption spectra of measured MRSI signal with large residual water peak for two voxels. (c)–(d) Absorption spectrum of the water-suppressed signal (blue) using the Löwner method and the quantified signal (red) in the two corresponding voxels. (e)–(f) Absorption spectrum of the water-suppressed signal using HSVD method and the quantified signal (red) in the two corresponding voxels. (g)–(h) Absorption spectrum of the water-suppressed signal using the Hankel-tensor method and the quantified signal (red) in the two corresponding voxels.

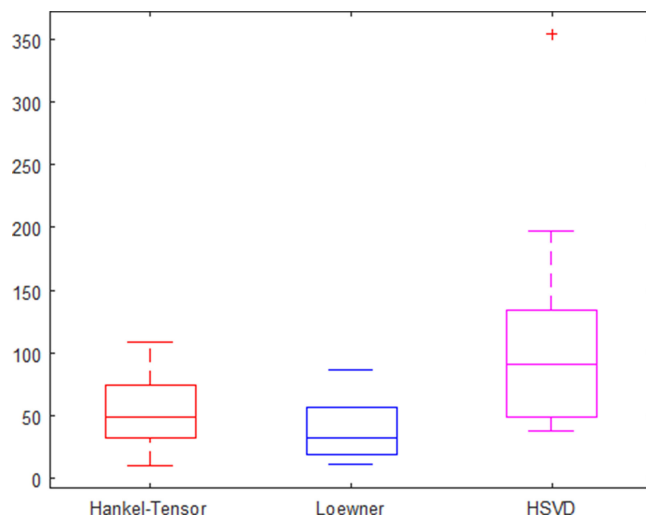


Fig. 7. Boxplots of error after residual water suppression using the methods HSVD, Löwner, and Hankel-tensor in 28 in-vivo MRSI signals. The error is calculated as the difference between the variance in water region segment and the variance from a segment in the noise region.

measured from brain tumor patients with a grid size 16×16 were used in this analysis. A band of three voxels at the outer edges of the MRSI grid were omitted to avoid chemical shift displacement artefacts and bad quality spectra. This resulted in a reduced MRSI grid size of 10×10 . AQSES [36] was used to quantify the MRSI signal in Matlab based SPID software [15]. An in-vitro basis set consisting of two lipids (Lip1 and Lip2), phosphocholine (PCh), Cre, Glu, glutamine (Gln), MI, Lac, N-Acetyl-Aspartate (NAA) and glycine (Gly) metabolites was used in the AQSES algorithm. Table I shows the average Cramer Rao bounds in % of quantified amplitude of five metabolites

TABLE I

MEAN AND STANDARD DEVIATION OF CRAMER RAO BOUNDS IN % OF QUANTIFIED AMPLITUDE FOR LIPID (LIP1), GLUTAMATE, N-ACETYLASPARTATE (NAA), AND PHOSPHOCHOLINE (PCh) METABOLITES OVER 10×10 MRSI VOXEL GRID

Patient-1						
	Mean			Standard deviation		
	HSVD	Hankel-tensor	Löwner-tensor	HSVD	Hankel-tensor	Löwner-tensor
Lipid	19.7016	21.1315	19.9462	11.7981	12.5221	12.2064
Glutamate	22.5448	25.9515	21.2197	9.7971	8.9112	9.3843
NAA	9.5400	10.9208	9.3868	4.3972	5.5443	4.0182
PCh	9.5269	9.7131	9.3248	3.4515	2.7612	3.1800
Patient-2						
	Mean			Standard deviation		
	HSVD	Hankel-tensor	Löwner-tensor	HSVD	Hankel-tensor	Löwner-tensor
Lipid	511.8554	51.7515	46.8847	4693.97	91.6301	86.9021
Glutamate	37.1549	38.1211	27.5632	29.6739	21.7350	12.5496
NAA	13.1994	14.7912	13.3217	4.5156	5.4552	4.4907
PCh	14.9876	14.1948	15.0810	8.9005	9.0866	12.4655

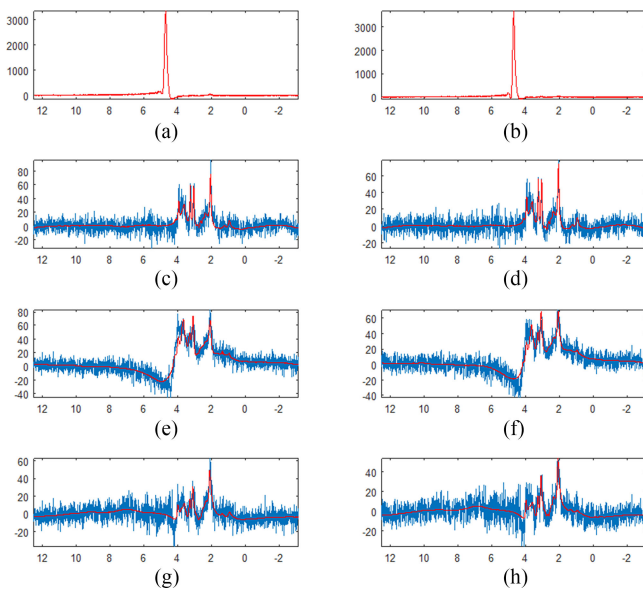


Fig. 8. Improper water suppression using the HSVD method in two voxels of the 10×10 MRSI grid. (a)–(b) Absorption spectra of measured MRSI signal with large residual water peak for two voxels. (c)–(d) Absorption spectrum of the water-suppressed signal (blue) using the Löwner method and the quantified signal (red) in the two corresponding voxels. (e)–(f) Absorption spectrum of the water-suppressed signal using HSVD method and the quantified signal (red) in the two corresponding voxels. (g)–(h) Absorption spectrum of the water-suppressed signal using the Hankel-tensor method and the quantified signal (red) in the two corresponding voxels.

along with the standard deviation for two of the in-vivo MRSI signals. In the first patient all three methods perform well and the average Cramer Rao bounds are similar. However, for the second patient the metabolites estimated from the MRSI signals after water suppression using HSVD clearly show higher Cramer Rao bounds for Glutamate and lipid metabolites because the HSVD method fails to suppress the water signal properly in many of the voxels as shown in Fig. 8. From Fig. 8, we can clearly see that the improper suppression the water signal will result in bad quantification of metabolites such as Glutamate. Even though the suppression of the water signal in two of those voxels using Hankel tensor is better than using HSVD, the quantification is not good compared to Löwner water suppression.

V. DISCUSSION

Residual water suppression is one of the common preprocessing steps used in the quantification of MRSI signals. T. Sundin *et al.* [10] propose a maximum-phase finite impulse response filter for residual water suppression. This method will alter the amplitude and phase of the filtered signal, which may create problems in quantification methods where different phase variations are not allowed and where spectra instead of quantified metabolites are used for the analysis [37], [38]. HSVD is the most widely used method and is available as a preprocessing step in many MRSI software packages. As it is applied on a voxel-by-voxel basis and as it computes the water source components separately for each voxel, it does not exploit the information shared among the voxels in the MRSI grid. Therefore, the HSVD method can fail to suppress water completely in a particular voxel due to noise or artifacts present in that voxel. This problem can be seen in an in-vivo example shown in Fig. 6 where the HSVD method fails to suppress the water in a particular voxel (Fig. 6(f)) and performs better in another voxel (Fig. 6(e)). This has motivated us to develop a new algorithm, which can exploit the similarity in water sources present among all voxels.

In this paper, we have represented the second-order MRSI data using a third-order tensor by means of a Löwner transform. A novel residual water-suppression method based on CPD, where sources are shared among many voxels, was developed. This work explored the feasibility and efficiency of the proposed algorithm in suppressing the residual water from MRSI data using both simulation and in-vivo signals. The Löwner-based method is applied simultaneously on the entire MRSI grid to estimate a large number of sources which can be used, in various combinations, to model the water component in each voxel. The water signal in each voxel is estimated as a linear combination of the sources with different voxel specific weights. This helps in preventing the failure of the water suppression in single voxels. The Löwner tensor is constructed using truncated spectra. Only the parts where the metabolite and water peaks are present are retained in the spectra. This helps in reducing the size of the tensor and the computational complexity of the algorithm without any significant impact on water suppression quality. The Löwner-based method requires fewer parameters

to model the water signal in the MRSI grid. For example, in the HSVD method with a rank-50, for each voxel we estimate 50 complex amplitude + 50 complex poles. For an MRSI grid of 8×8 the total number of free parameters includes 50×64 complex amplitudes and 50×64 complex poles. In case of the Löwner method with a rank-50 and polynomial degree 4, the total number of free parameters for an MRSI grid of 8×8 include 50 complex poles + 54×64 complex amplitudes.

When using the Löwner method to estimate the water sources we have applied the CPD only on the compressed core tensor S and the factor matrices are obtained as explained in the Section II-A. It speeds up the algorithm without any significant negative consequences in the estimated water signal. In general, the factor matrices obtained from the compressed CPD step are typically used as the initial values in the computation of the CPD of the full tensor to further improve the decomposition, also known as the refinement step. Here, we have not used the refinement step as it is computationally intensive and did not provide any significant improvement in the estimated water signal. In the Löwner-based method we have added a quality verification on the water suppression to overcome the problems with random initialization. If the algorithm is used with different initializations to obtain a better water suppression, the compression step is only performed once as it is deterministic. Since the compression step takes most of the computation time and the CPD on the core tensor is relatively fast, running the algorithm again with a different initialization will not increase the computation significantly. A rank $R = 50$ was used for the CPD of the Löwner tensor \mathcal{L}_S based on the assumption that the water signal from all the voxels can be modelled using 20–25 first-order rational functions and the remaining ones are sufficient to model the metabolites. The chosen rank was not sensitive to the grid size in the sense that similar performance was obtained on the larger voxel grid (16×16) as well as on the smaller voxel grid (8×8). Also, the selection of the rank itself is not so sensitive since the results did not change significantly when increasing (e.g., $R = 60$) or decreasing the rank (e.g., $R = 40$).

The Hankel-tensor based method has been used to estimate the parameters of exponentially damped sinusoids of multichannel signals [31]. In this paper we have used the Hankel-tensor based method as a natural extension of the HSVD method to estimate the water signals from MRSI data. The Hankel-tensor method has better performance compared to the HSVD method in both simulations and in-vivo data, however its performance is still worse than the Löwner method. Both Hankel-tensor and HSVD methods extract sources with broad peaks, which helps in tackling the baseline without the need for additional polynomial sources. A higher model-order (rank) of 100 was used, as the performance deteriorated when a model order similar to the HSVD-rank (50) was used. The reason is that a rank of 50 is typically sufficient for modelling a signal from an individual voxel, but is not sufficient to capture all the variations in damping and frequency shifts across signals in the MRSI grid. The Hankel tensor requires a higher model order (rank) compared to the Löwner method because the frequency domain decouples the noise, artefacts and trends present outside the region of interest and also a higher rank was needed to model the variations in trend across different voxels. The Hankel-tensor was

constructed using the entire FID signal of length 2048, which resulted in a large tensor and higher computational complexity. A truncated FID (<2048 samples) can also be used to construct the Hankel-tensor to reduce the size and complexity, but its performance is worse than HSVD in in-vivo MRSI data.

All three methods model the total MRS signal sufficiently well, however in some voxels HSVD fails to suppress the water completely. This happens mainly because the water signal is modeled from the sources whose frequencies are outside the region of interest (0.25–4.2 ppm) and in some cases (e.g., Fig. 6) part of the water signal is modelled by a few sources whose frequencies lie in the region of interest (0.25–4.2 ppm). Therefore, a small residual water is present in the water suppressed signal, since part of the water signal modelled by sources in the region of interest (0.25–4.2 ppm) is not subtracted.

As a proof of concept, we have analyzed the proposed methods in terms of residual error in case of simulation and difference in variance for in-vivo examples. Also, we have assessed the water suppression quality of three methods using the average Cramér-Rao bounds of the metabolite amplitude in two in-vivo patients. Although Cramér-Rao bounds depend on more factors, they are often used in in-vivo studies to assess the reliability of metabolite quantification. In the future, these water suppression methods could also be compared in terms of reliability of metabolite quantification in a test-retest experiment.

VI. CONCLUSION

A tensor-based method which suppresses residual water simultaneously in all MRSI voxels using a Löwner-based blind source separation technique and Hankel-tensor based exponential data-fitting technique are proposed. These methods were tested on both simulated and in-vivo ^1H MRSI signals. In both cases the tensor-based methods perform better than the widely-used subspace-based HSVD method, which uses a single Hankel matrix from one spectrum at a time. Comparing the two tensor-based methods, the Löwner-tensor based method was shown to better suppress residual water in MRSI. The main advantage of Löwner-based method is that it can handle presence of artifacts in some voxels without significantly affecting the water suppression quality. In contrast, the HSVD method completely fails to suppress water in some voxels when artifacts are present, thus making the further analysis of those spectra difficult.

ACKNOWLEDGMENT

The authors would like to thank the University Hospitals of Leuven for data acquisition.

REFERENCES

- [1] S. R. Dager *et al.*, "Research applications of magnetic resonance spectroscopy (MRS) to investigate psychiatric disorders," *Topics Magn. Reson. Imag.*, vol. 19, no. 2, pp. 81–96, 2008.
- [2] F. S. De Edelenyi *et al.*, "Application of independent component analysis to ^1H MR spectroscopic imaging exams of brain tumours," *Analytica Chimica Acta*, vol. 544, no. 1, pp. 36–46, 2005.
- [3] S. Van Cauter *et al.*, "Integrating diffusion kurtosis imaging, dynamic susceptibility-weighted contrast-enhanced MRI, and short echo time chemical shift imaging for grading gliomas," *Neuro-oncology*, vol. 16, no. 7, pp. 1010–1021, 2014.

- [4] P. J. Bolan *et al.*, "Imaging in breast cancer: Magnetic resonance spectroscopy," *Breast Cancer Res.*, vol. 7, no. 4, pp. 149–152, 2005.
- [5] S. Friedman *et al.*, "Regional brain chemical alterations in young children with autism spectrum disorder," *Neurology*, vol. 60, no. 1, pp. 100–107, 2003.
- [6] R. J. Ogg *et al.*, "WET, a T1- and B1-insensitive water-suppression method for in vivo localized ^1H NMR spectroscopy," *J. Magn. Reson., Ser. B*, vol. 104, no. 1, pp. 1–10, 1994.
- [7] H. Barkhuijsen *et al.*, "Improved algorithm for noniterative time-domain model fitting to exponentially damped magnetic resonance signals," *J. Magn. Reson.*, vol. 73, no. 3, pp. 553–557, 1987.
- [8] E. Cabanes *et al.*, "Optimization of residual water signal removal by HLSVD on simulated short echo time proton MR spectra of the human brain," *J. Magn. Reson.*, vol. 150, no. 2, pp. 116–125, 2001.
- [9] L. Vanhamme *et al.*, "Fast removal of residual water in proton spectra," *J. Magn. Reson.*, vol. 132, no. 2, pp. 197–203, 1998.
- [10] T. Sundin *et al.*, "Accurate quantification of ^1H spectra: From finite impulse response filter design for solvent suppression to parameter estimation," *J. Magn. Reson.*, vol. 139, no. 2, pp. 189–204, 1999.
- [11] M. Wilson *et al.*, "A constrained least-squares approach to the automated quantitation of in vivo ^1H magnetic resonance spectroscopy data," *Magn. Reson. Med.*, vol. 65, no. 1, pp. 1–12, 2011.
- [12] C. Ma *et al.*, "Removal of nuisance signals from limited and sparse 1h MRSI data using a union-of-subspaces model," *Magn. Reson. Med.*, vol. 75, no. 2, pp. 488–497, 2016.
- [13] Z. Dong, "Proton MRS and MRSI of the brain without water suppression," *Prog. Nucl. Magn. Reson. Spectrosc.*, vol. 86, pp. 65–79, 2015.
- [14] D. Stefan *et al.*, "Quantitation of magnetic resonance spectroscopy signals: The jMRUI software package," *Meas. Sci. Technol.*, vol. 20, no. 10, 2009, Art. no. 104035.
- [15] J. B. Pouillet, "Quantification and classification of magnetic resonance spectroscopic data for brain tumor diagnosis," Ph.D. dissertation, Dept. Elect. Eng., KU Leuven, Leuven, Belgium, 2008.
- [16] B. Soher *et al.*, "VeSPA: Integrated applications for RF pulse design, spectral simulation and MRS data analysis," in *Proc. 19th Annu. Meeting Int. Soc. Magn. Reson. Med.*, 2011, p. 1410.
- [17] O. Debals *et al.*, "Löwner-based blind signal separation of rational functions with applications," *IEEE Trans. Signal Process.*, vol. 64, no. 8, pp. 1909–1918, Apr. 2016.
- [18] A. Cichocki *et al.*, "Tensor decompositions for signal processing applications: From two-way to multiway component analysis," *IEEE Signal Process. Mag.*, vol. 32, no. 2, pp. 145–163, Mar. 2015.
- [19] N. Sidiropoulos *et al.*, "Tensor decomposition for signal processing and machine learning," *IEEE Trans. Signal Process.*, vol. 65, no. 13, pp. 3551–3582, Jul. 2017.
- [20] I. Domanov and L. De Lathauwer, "On the uniqueness of the canonical polyadic decomposition of third-order tensors—Part I: Basic results and uniqueness of one factor matrix," *SIAM J. Matrix Anal. Appl.*, vol. 34, no. 3, pp. 855–875, 2013.
- [21] I. Domanov and L. De Lathauwer, "On the uniqueness of the canonical polyadic decomposition of third-order tensors—Part II: Uniqueness of the overall decomposition," *SIAM J. Matrix Anal. Appl.*, vol. 34, no. 3, pp. 876–903, 2013.
- [22] L. De Lathauwer *et al.*, "On the best rank-1 and rank- (R_1, R_2, \dots, R_n) approximation of higher-order tensors," *SIAM J. Matrix Anal. Appl.*, vol. 21, no. 4, pp. 1324–1342, 2000.
- [23] L. De Lathauwer *et al.*, "A multilinear singular value decomposition," *SIAM J. Matrix Anal. Appl.*, vol. 21, no. 4, pp. 1253–1278, 2000.
- [24] T. G. Kolda and B. W. Bader, "Tensor decompositions and applications," *SIAM Rev.*, vol. 51, no. 3, pp. 455–500, 2009.
- [25] E. Sanchez and B. R. Kowalski, "Tensorial resolution: A direct trilinear decomposition," *J. Chemometrics*, vol. 4, no. 1, pp. 29–45, 1990.
- [26] R. Bro and C. A. Andersson, "Improving the speed of multiway algorithms: Part II: Compression," *Chemometrics Intell. Lab. Syst.*, vol. 42, no. 1, pp. 105–113, 1998.
- [27] A. Antoulas and B. Anderson, "On the scalar rational interpolation problem," *IMA J. Math. Control Inf.*, vol. 3, no. 2/3, pp. 61–88, 1986.
- [28] T. Antoulas, "A tutorial introduction to the Loewner framework for model reduction," in *Proc. 9th Elgersburg Workshop Mathematische Systemtheorie*, 2014, pp. 1–54.
- [29] K. Löwner, "Über monotone matrixfunktionen," *Mathematische Zeitschrift*, vol. 38, no. 1, pp. 177–216, 1934.
- [30] I. Domanov and L. De Lathauwer, "Generic uniqueness of a structured matrix factorization and applications in blind source separation," *IEEE J. Sel. Topics Signal Process.*, vol. 10, no. 4, pp. 701–711, Jun. 2016.
- [31] J.-M. Papy *et al.*, "Exponential data fitting using multilinear algebra: The single-channel and multichannel case," *Numer. Linear Algebra Appl.*, vol. 12, no. 8, pp. 809–826, 2005.
- [32] N. Vervliet *et al.*, Tensorlab 3.0, Mar. 2016. [Online]. Available: <http://www.tensorlab.net>
- [33] N. Vervliet *et al.*, "Tensorlab 3.0—Numerical optimization strategies for large-scale constrained and coupled matrix/tensor factorization," ESAT-SISTA, KU Leuven, Leuven, Belgium, Tech. Rep. 16–173, 2016.
- [34] S. Van Cauter *et al.*, "Reproducibility of rapid short echo time CSI at 3 Tesla for clinical applications," *J. Magn. Reson. Imag.*, vol. 37, no. 2, pp. 445–456, 2013.
- [35] M. I. Osorio Garcia, "Advanced signal processing for magnetic resonance spectroscopy," Ph.D. dissertation, Dept. Elect. Eng., KU Leuven, Leuven, Belgium, 2011.
- [36] J.-B. Pouillet *et al.*, "An automated quantitation of short echo time MRS spectra in an open source software environment: Aqsqs," *NMR Biomed.*, vol. 20, no. 5, pp. 493–504, 2007.
- [37] H. N. Bharath *et al.*, "Nonnegative canonical polyadic decomposition for tissue-type differentiation in gliomas," *IEEE J. Biomed. Health Inform.*, vol. 21, no. 4, pp. 1124–1132, Jul. 2017.
- [38] Y. Li *et al.*, "Hierarchical nonnegative matrix factorization (hNMF): A tissue pattern differentiation method for glioblastoma multiforme diagnosis using MRSI," *NMR Biomed.*, vol. 26, no. 3, pp. 307–319, 2013.